Ag-Organic Layered Samples for Optoelectronic Applications: Interface Width and Roughening Using a 500 eV Cs+ Probe in Dynamic Secondary Ion Mass Spectrometry

ARTICLE *in* ANALYTICAL CHEMISTRY · DECEMBER 2012

Impact Factor: 5.64 · DOI: 10.1021/ac302939m · Source: PubMed

5 AUTHORS, INCLUDING:

Patrick Philipp
Luxembourg Institute of Science and Technol…
43 PUBLICATIONS **189** CITATIONS
SEE PROFILE

Max Shtein
University of Michigan
86 PUBLICATIONS **2,554** CITATIONS
SEE PROFILE

John Kieffer
University of Michigan
138 PUBLICATIONS **1,427** CITATIONS
SEE PROFILE

Tom Wirtz
Luxembourg Institute of Science and Technol…
94 PUBLICATIONS **569** CITATIONS
SEE PROFILE

analytical chemistry

Article

pubs.acs.org/ac

Ag-Organic Layered Samples for Optoelectronic Applications: Interface Width and Roughening Using a 500 eV Cs^+ Probe in Dynamic Secondary Ion Mass Spectrometry

Patrick Philipp,*[,†] Quyen K. Ngo,*[,†] Max Shtein,[‡] John Kieffer,[‡] and Tom Wirtz[†]

[†]Department "Science and Analysis of Materials" (SAM), Centre de Recherche Public−Gabriel Lippmann, 41 Rue du Brill, L-4422 Belvaux, Luxembourg

[‡]Department of Materials Science and Engineering, University of Michigan, Ann Arbor, Michigan 48109-2136, United States

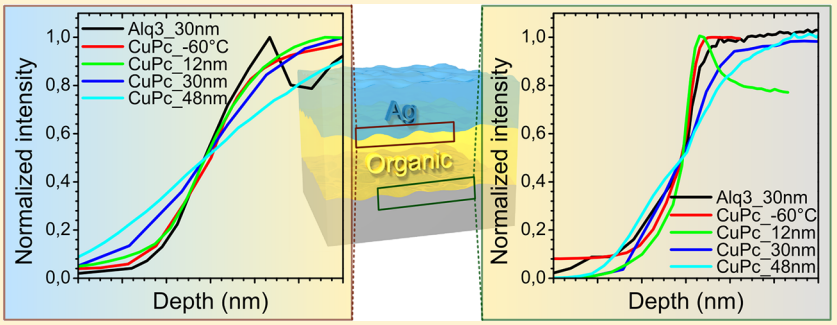

ABSTRACT: The performance of organic optoelectronic devices depends a lot on interface structure and width. Dynamic secondary ion mass spectrometry (SIMS) has been widely used to investigate interfaces in classical semiconductor devices and limitations are quite well understood. For low-energy dynamic SIMS on organic optoelectronic devices, sputter-induced diffusion processes and roughness formation have only been investigated sparsely. In this work we use low-energy dynamic SIMS depth profiling on metal−organic multilayered model samples with compositions similar to organic optoelectronic devices to investigate limitations in the calculation of interface widths due to sputter-induced roughness formation. The samples consist of silver and organic compounds (e.g., tris(8-hydroxyquinolinato) aluminum (Alq_3) and metal phthalocyanines) sequentially deposited by thermal evaporation in vacuum onto a Si substrate. They are analyzed by a 500 eV Cs^+ primary ion beam. Surface roughness at the SIMS crater bottoms is characterized by AFM as a function of crater depth. We find that the roughness in SIMS craters is limited to approximately 1.5 nm, which is much smaller than the interface width of the as-deposited interfaces. Thus, for the studied organic−inorganic interfaces, low-energy dynamic SIMS can yield accurate information about interface morphology, allowing the study of its dependence on sample preparation conditions and its implication on device properties.

Recently, the increasing sophistication of organic optoelectronic devices (e.g., organic light-emitting diodes and organic photovoltaic cells, etc.) requires molecular-level dimensional control in the fabrication of multilayered structures with specifically engineered interfaces. Various processing approaches, conditions, and material combinations (e.g., metal evaporated onto an organic film) can result in nonflat interfaces, which can significantly affect device properties. Knowing precisely the morphology of an interface can help better understand and control the processing-structure−property relationship for this class of devices.

Among various analytical techniques that can yield information about interfacial morphology, like scanning electron microscopy (SEM), atomic force microscopy (AFM), cross-sectional transmission electron microscopy (XTEM), and small-angle X-ray diffraction (SAXD), secondary ion mass spectrometry (SIMS) can be a convenient and powerful technique, allowing one not only to obtain information about molecular, elemental, and isotopic composition of surfaces[1] but also to carry out depth profiling[2] and contamination monitoring.[3] Classically, SIMS depth profiling was mainly focusing on inorganic samples. Depth profiling of organic matter was hampered for a long time by the significant fragmentation caused by energetic monatomic ions, i.e., the molecular information gets lost during the sputtering. Recent studies have shown that SIMS depth profiling can be successful in some situations by using polyatomic or cluster ion bombardment.[4,5] A large variety of different clusters have been studied: C_{60}^{n+},[6−12] Au_n^{q+} ($5 \le n \le 400$, $1 \le q \le 4$),[13−17] SF_5^+,[18,19] Bi_n^+,[20] as well as Ar_n^+ (n = 500−2000).[21−23] When a cluster ion impacts on a surface, every atom of the cluster has only a fraction of the initial energy of the whole cluster. As a result, this significantly lowers the penetration depth, reduces fragmentation of the organic molecules and maintains the chemical structure in the impact region, and enhances the

Received: October 10, 2012
Accepted: December 3, 2012
Published: December 3, 2012

secondary ion yield. Shard et al.[7] studied alternating layers of vacuum evaporated Irganox1010 (2.5 nm) and Irganox3114 (55 or 90 nm) by a C_{60}^{n+} primary ion beam with impact energies of 5 and 10 keV (C_{60}^{+}), 20 keV (C_{60}^{2+}), and 30 keV (C_{60}^{3+}) impact energies. In this study, the depth resolution was worse than 2.5 nm, and it was limited by the development of roughness in the irradiated area. Lee et al. investigated an organic delta-layered sample (Irganox 3114 layer of ∼2.4 nm embedded between Irganox 1010 layers with thicknesses of ∼46 nm for the first two layers and ∼96 nm for the subsequent three layers) using a massive Ar cluster ion beam (mean cluster sizes of 500−1000 atoms).[23] Taking the evolution of surface topography adequately into account proved to be a problem: the roughness was 0.3 nm for the nonirradiated surface and it increased up to 5 nm during sputtering. Hence, up until now, cluster beams cannot match the depth resolutions achieved by low-energy monatomic ion bombardment necessary to characterize the interfaces in organic optoelectronic devices.

Along with depth profiling by cluster ions, low energy ion beams were introduced for depth profiling. Examples described in the literature include multiquantum wells Ge delta-doped Si sample,[24] PMMA-C_{60} blends,[25] organic light-emitting diodes model of Ag/Alq_3/NPB/ITO,[26] tetraphenylporphyrins (H2TPP and ZnTPP) and phthalocyanines organic superlattices,[27] and polycarbonate (PC).[28] For the characterization of organic samples, the low-energy atomic bombardment causes less fragmentation than sputtering by high energy atoms, and therefore some organic fragments can be observed throughout the depth profiles.[25,28,29] However, none of the previous papers investigated the evolution of roughness as a function of crater depth nor how it may affect the characterization of interfaces and the interface widths calculated from SIMS depth profiles in particular. In organic optoelectronic devices, this interface structure has however an impact on interface heat conduction, i.e., for thinner multilayered films mixing of phases at interfaces occurs and leads to decreased thermal boundary resistance.[30] In addition, a rough metal electrode scatters plasmons more efficiently and enhances the emission intensity of OLEDs.[31]

In the present study, limitations in interface characterization due to roughness formation as a function of crater depth will be investigated. We optimize conditions for the low-energy Cs^+ depth profiling of metal−organic interfaces of a series of bilayered samples presenting a silver and an organic layer on silicon and compare the SIMS-deduced interface resolution to RMS roughness measured by AFM in the SIMS craters. The analysis of the metal−organic multilayered systems by low-energy dynamic SIMS yields new interesting results. The different organic layers can be distinguished in SIMS depth profiles down to the nanometer scale, an important capability for characterizing the structure of typical optoelectronic devices. Moreover, the use of sample rotation during SIMS analysis can reduce irradiation-induced roughness and thus enhances depth resolution similar to inorganic samples.[32]

EXPERIMENTAL SECTION

The samples used in this study comprise thin films of silver and organic semiconductor compounds deposited onto silicon by vacuum thermal evaporation onto silicon at room temperature, unless otherwise noted. The organic molecules are phthalocyanine derivatives ($C_{32}H_{16}N_8Cu$, named CuPc) and aluminum tris(8-hydroxyquinoline) ($C_{27}H_{18}N_3O_3Al$, named Alq_3). The samples were prepared at a pressure of approximately 10^{-6} mbar using a commercial deposition system (Angstrom Engineering AMod) and a custom superlattice deposition system. The silicon substrates were cleaned by sonicating in detergent, acetone, trichloroethylene, and isopropanol before deposition. During the deposition process, the film thickness was monitored using a precalibrated quartz crystal microbalance. For precalibration, ellipsometry was used. The monitored film thicknesses were used to convert the time scale of the SIMS depth profiles into a depth scale. In each sample, the Ag and organic layers have the same thickness. The samples are described in Table 1.

Table 1. List of Samples and Preparation Conditions

name	sample	layer thickness (nm)	deposition system	deposition temperature
Alq3_30	Ag/Alq3	30	Angstrom	room temperature
CuPc_30	Ag/CuPc	30	Angstrom	room temperature
CuPc_−60 °C	Ag/CuPc	13	Angstrom	−60 °C
CuPc_12	Ag/CuPc	12	Superlattice	room temperature
CuPc_48	Ag/CuPc	48	Superlattice	room temperature

The SIMS experiments were carried out using a Cs^+ primary ion beam at an impact energy of 500 eV in the positive and the negative secondary ion mode on a Cameca SC-Ultra instrument. For some samples in the negative secondary ion mode, depth profiles were carried out with and without sample rotation, for the other conditions no sample rotation was used. The sample voltage was set to −2 kV and −3 kV in the negative mode and to 3 kV in the positive mode. The incidence angle with respect to the sample normal is about 46° in the negative mode and about 64° in the positive mode. These angles are instrument-dependent and cannot be changed. At first, for each sample, a depth profile throughout the different layers down to the substrate was obtained. Then, using the same conditions, craters were prepared for subsequent AFM characterization by stopping the sputtering at certain depths (e.g., at the Ag/organic interface, in the middle of the organic layer, and at the organic/Si interface). The primary ion current ranged between 3 and 20 nA. The mass resolution $M/\Delta M$ was maintained at 400. A contrast aperture of 300 μm was used, and the energy slit was closed to a width of 45 eV. The raster size was set to 300 × 300 μm^2, and the field aperture had a diameter of 1200 μm.

The surface roughness in the sputtered craters was measured on a Molecular Imaging PicoSPM LE AFM instrument in ambient air. The images were recorded using the tapping mode with a scanning area of 5 × 5 μm^2 and with an image resolution of 512 × 512 pixels. For craters sputtered into the CuPc layer, the AFM images exhibited a number of high hillocks. As described in a previous paper,[33] these hillocks appear only in the SIMS craters after exposure to air and are formed by cesium oxide droplets. They are not present in vacuum and should not be considered for the calculation of surface roughness.[33] Therefore, the hillocks are masked out when calculating the RMS roughness (Figure 1).

RESULTS AND DISCUSSION

Depth Profiles. The fragmentation of CuPc and Alq_3 molecules under low-energy Cs^+ bombardment has been

dx.doi.org/10.1021/ac302939m | Anal. Chem. 2013, 85, 381−388

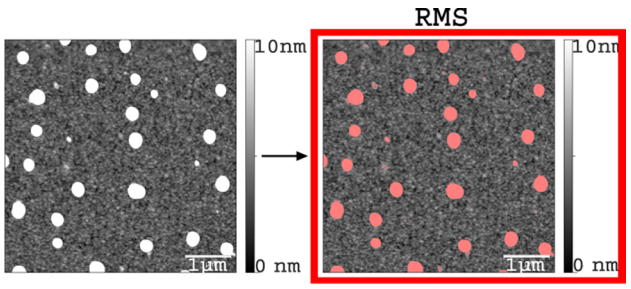

Figure 1. Example showing Cs−O droplets that are masked for the calculation of the RMS roughness in the SIMS craters.

described in a previous paper.[34] For depth profiling, we selected a characteristic fragment of the organic layers leading to high secondary ion yields, i.e., CN^- at m/z = 26. The inorganic layers are characterized by Ag^- (m/z = 107) and Si^- (m/z = 28) intensities. Mass interferences for the different fragments have been checked and have been found to be a few orders of magnitude below the intensities in the different layers and thus of no major concern.

Figure 2 compares the depth profiles recorded in the negative mode for the samples Alq_3_30 nm, CuPc_30 nm, CuPc_12 nm, and CuPc_48 nm. The interfaces have been positioned at 50% of the maximum secondary ion intensity inside a given layer. All depth profiles show similar properties. The organic layers are characterized by high intensities of

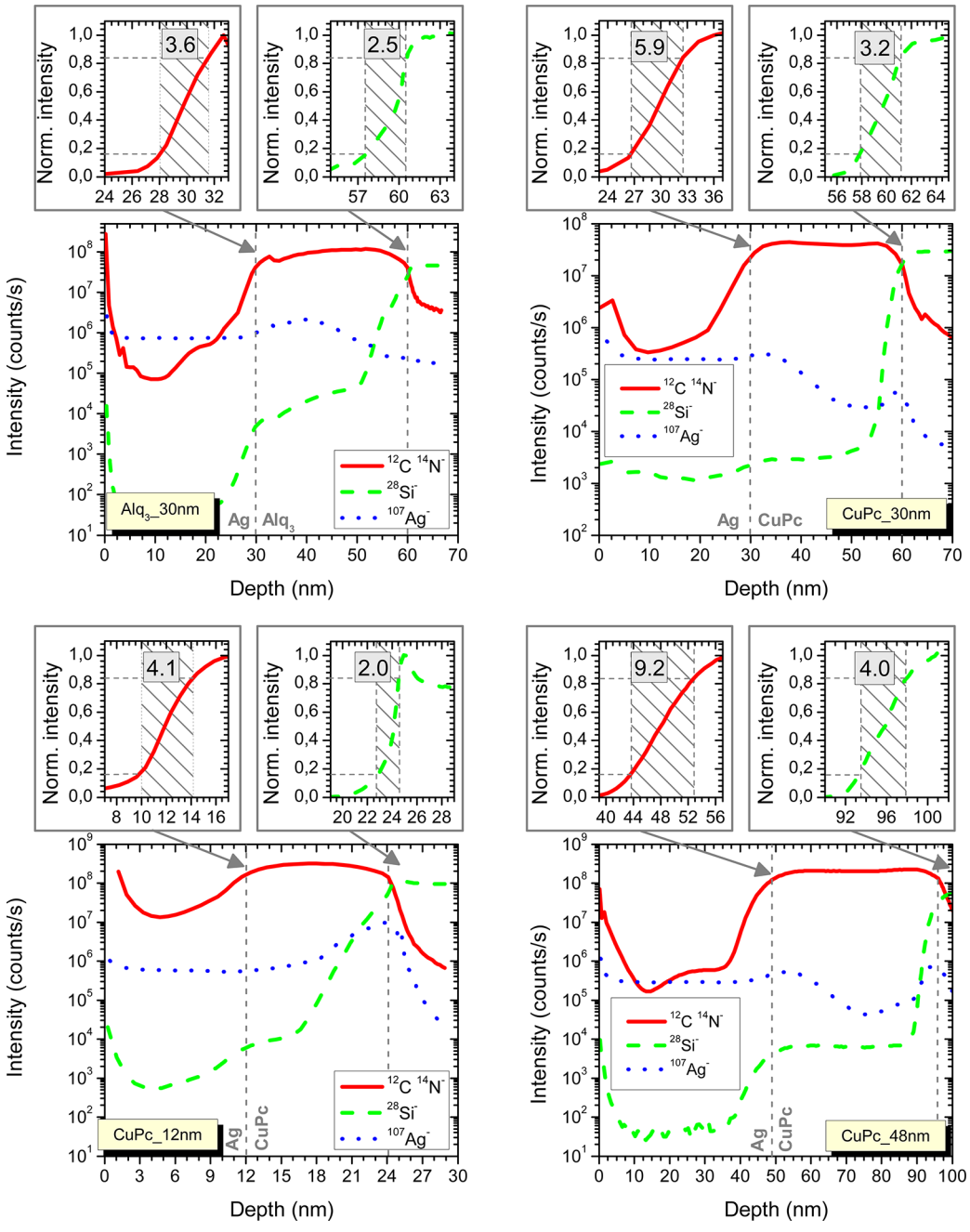

Figure 2. Secondary ion intensities as a function of depth in Cs^+ low-energy depth profiles of the samples Alq_3_30 nm, CuPc_30 nm, CuPc_12 nm, and CuPc_48 nm. Interface widths for the CN^- and Si^- intensities are shown in the insets with a linear scale.

dx.doi.org/10.1021/ac302939m | *Anal. Chem.* 2013, 85, 381−388

$^{12}C^{14}N^-$ cluster ions. High intensities of the same cluster ion in the Ag layer are due to mass interferences caused by residual gas in the analysis chamber. The Si substrate is characterized by $^{28}Si^-$ intensities exceeding 10^7 counts/s. An increase of the $^{28}Si^-$ intensities above 10^3 counts/s when passing the Ag/organic interfaces are caused by mass interferences with secondary ion clusters containing C, N, H, and O originating from the CuPc and Alq_3 molecules. A higher O concentration in Alq_3 explains the higher intensities at m/z = 28 in the Alq_3 layer of the Alq_3_30 nm sample. The observations from the previous samples remain valid for sample CuPc_−60 °C which has been prepared using a substrate cooled to −60 °C (Figure 3).

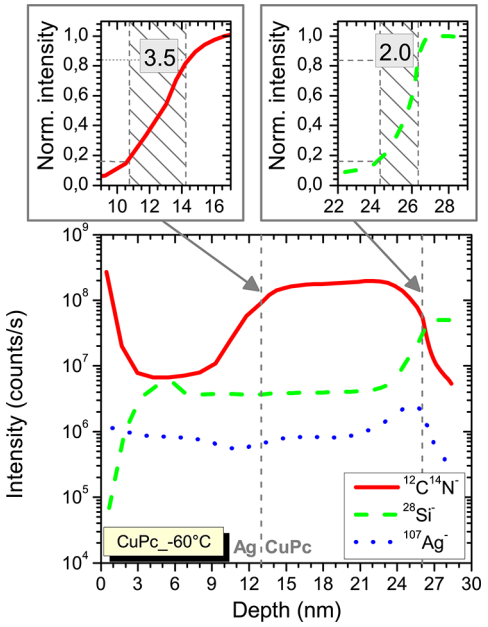

Figure 3. Secondary ion intensities as a function of depth in Cs^+ low-energy depth profiles of the sample CuPc_−60 °C.

In all depth profiles, secondary ion intensities for m/z = 107 are high in the different organic layers (Figures 2 and 3). They are caused by Ag diffusion into the organic layer either during the deposition process or during the SIMS analysis or by a combination of the two mechanisms. Diffusion during SIMS analysis would complicate the interpretation of the $^{107}Ag^-$ secondary ion intensities but has already been observed for other elements in semiconductor samples.[35] In our samples, irradiation-induced diffusion contributes most probably to the diffusion profile, especially as the Ag diffusion is also clearly visible in the CuPc sample cooled down to −60 °C during the deposition process (Figure 3). Some study on these processes along with methods used to identify the origin of the diffusion processes will be presented in a separate paper.

The interface widths have been calculated using the distance between 84% and 16% of the secondary ion intensities at the rising edge of the $^{12}C^{14}N^-$ intensities for the Ag/organic interfaces and of the $^{28}Si^-$ intensities for the organic/Si interfaces. Normally, depth resolutions in SIMS are calculated using the falling edge of the depth profiles because it represents well sputter-induced mechanisms.[36] In this work we want to estimate the interface width at the different interfaces. Therefore, we calculate the interface resolutions using the rising edge of the depth profiles which is shown to be less influenced by the conditions of primary ion bombardment, and thus closer to the real interface width than those calculated from the falling edge.[37]

The interface width calculated for the different samples is shown in the insets with the linear scale zooming in the interface regions (Figures 2 and 3). For each sample, the interface width at the organic/Si interface is smaller than the value of the Ag/organic interface. This is expected as the silicon wafers used for sample preparation have a small surface roughness close to 0.1 nm,[38,39] and interface broadening is either due to atomic mixing or roughness formation during the sputtering of the Ag and organic layers. For the Ag/organic interface, several comparisons can be made. For identical preparation conditions and the same layer thicknesses, the Alq_3 sample presents a smaller interface width than the CuPc sample (3.6 nm for the Alq_3_30 nm vs 5.9 nm for the CuPc_30 nm sample). At this stage, the increased interface width could also be due to increased roughness formation during SIMS depth profiling, which will be checked in the next section. Reducing the temperature during the deposition process leads to a smaller interface width of 3.5 nm for the CuPc_−60 °C sample compared to 5.9 nm for the CuPc_30 nm sample. The interface width is also sensitive to the layer thickness. Sample CuPc_12 nm has a significantly smaller interface width (4.1 nm) than sample CuPc_48 nm (interface width of 9.2 nm). At the same time, the interface width of these samples for a similar film thickness seems to be slightly higher than for sample CuPc_30 nm prepared on another instrument. Thus, for a same molecule, the interface thickness depends on sample preparation conditions. Besides, thicker films lead to larger interface widths. In addition, when cooling the substrate down to −60 °C during the deposition process, the Ag/organic interface width gets smallest (3.5 nm for sample CuPc_−60 °C compared to 4.1 nm for sample CuPc_12 nm).

For the CuPc_30 nm sample, the depth profile has also been carried out in the positive secondary ion mode using MCs^+ clusters, and interface widths are larger than in the negative mode: the Ag/CuPc interface has a width of 7.4 nm and the CuPc/Si interface a width of 3.9 nm. This can be related to increased roughness formation at the interfaces and will be presented in more detail in the next section.

Our study shows that the interface width depends on interface position, organic layer composition, and thickness as well as sample preparation method and conditions. For all depth profiles, the interface width at the organic/Si interface is smaller than at the Ag/organic interfaces. At the same time the Ag/organic interface width seems to increase for thicker Ag and organic layers, indicating that rougher interfaces and preferential sputter rates leading to roughness formation during SIMS analysis may influence it. This will be discussed in the next section.

According to the data presented here, low-energy SIMS depth profiling is successful in characterizing the interface roughness formed during sample preparation and can help to relate interface width to physical properties of organic optoelectronic devices. However, before final conclusions can be drawn, the interface widths calculated from the depth profiles need to be checked for any contribution from roughness developing during depth profiling, i.e., roughness in the SIMS crates must stay at every crater depth significantly below the values calculated for the interface widths.

Roughness at Interfaces. As mentioned in the previous section, the control of roughness at the SIMS crater bottoms at

dx.doi.org/10.1021/ac302939m | *Anal. Chem.* 2013, 85, 381−388

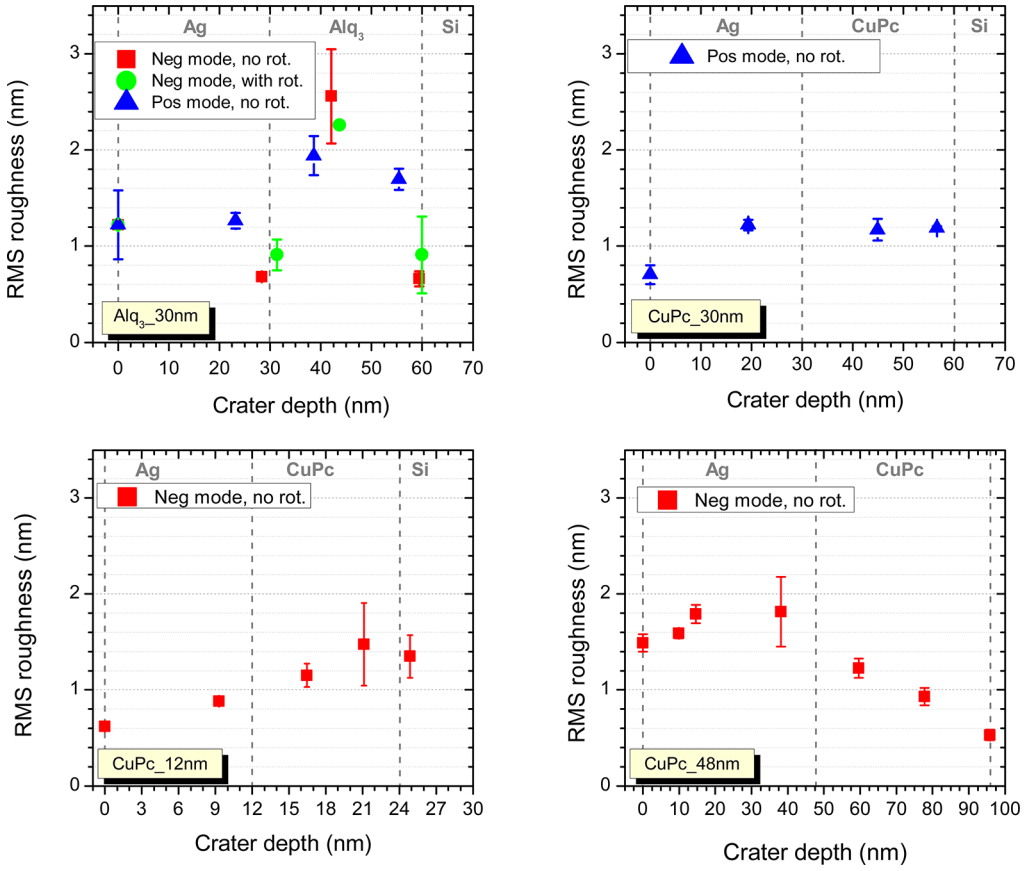

Figure 4. RMS roughness variation as a function of depth in low energy Cs^+ depth profiles of samples Alq_3_30 nm, CuPc_30 nm, CuPc_12 nm, and CuPc_48 nm.

every depth of the profiles is essential for the validity of the determined interface widths. In this section, the roughness is characterized at certain depths of the depth profiles shown in Figures 2 and 3. Figure 4 presents the evolution of the roughness for the samples Alq_3_30 nm, CuPc_30 nm, CuPc_12 nm, and CuPc_48 nm. The same data for the CuPc_−60 °C sample is shown in Figure 5. For the CuPc samples prepared at room temperature, roughness formation is only studied for the positive or the negative secondary ion mode, both without sample rotation. For the Alq_3 and the CuPc_−60 °C samples, negative and positive secondary ion modes have been investigated. Sample rotation is only used for the first mode.

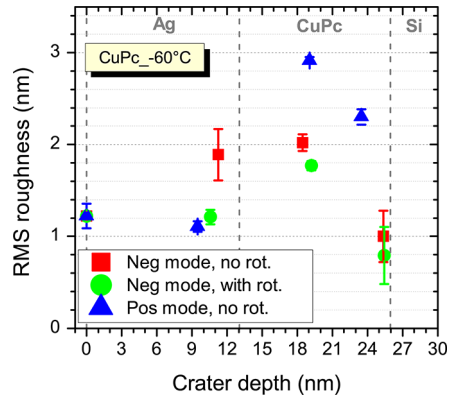

Figure 5. RMS roughness variation as a function of depth in low-energy Cs^+ depth profiles of sample CuPc_−60 °C.

For the craters sputtered using the negative secondary ion mode, the evolution of roughness depends on sample composition and layer thicknesses. For the Alq_3_30 nm sample, the surface roughness is reduced while sputtering the Ag layer. After sputtering half of the Alq_3 layer, the RMS roughness increases above 2.6 nm but reduces when coming close to the Alq_3/Si interface. At the interfaces, RMS values are equal to 0.7 nm. For this sample, the maximum roughness is partially reduced by using sample rotation during the sputtering of the craters. The maximum roughness in the middle of the Alq_3 layer reduces from 2.6 to 2.3 nm, and at the interfaces it is increased by about 0.2−0.9 nm. A similar behavior is observed for the CuPc_−60 °C sample in the negative secondary ion mode without sample rotation. The RMS roughness increases up to 1.9 nm close to the Ag/CuPc interface. In the organic layer, roughness increases even above 2 nm before getting lowered to 1 nm at the CuPc/Ag interface. For this sample, using sample rotation during the sputtering of the craters reduces roughness formation significantly, especially for the Ag/CuPc interface (roughness of 1.2 nm). The other values improve by about 0.2 nm (roughness of 1.8 and 0.8 nm). Overall, sample rotation was more successful on this sample than on the Alq_3_30 nm sample, where roughness could only be lowered by about 0.3 nm in the middle of the Alq_3 layer. At the interfaces, roughness was even slightly worse with sample rotation than without. For the CuPc_12 nm and CuPc_48 nm samples prepared at room temperature, the behavior changes. Roughness increases during the sputtering of the Ag layer, and

dx.doi.org/10.1021/ac302939m | Anal. Chem. 2013, 85, 381−388

this increase is highest for the thickest layer. It increases up to 1.1 nm for the CuPc_12 nm sample and up to 1.8 nm for the CuPc_48 nm sample. For the thinnest samples, roughness continues to increase in the CuPc layer (maximum roughness of 1.5 nm) and reduces only marginally at the CuPc/Si interface (roughness of 1.3 nm). Roughness decreases continuously down to 0.5 nm at the CuPc/Si interface for the CuPc_48 nm sample. The general trend observed is increasing roughness during the sputtering of the Ag layer for the CuPc samples and decreasing roughness in the same layer for the Alq_3_30 nm sample. The roughness at the organic/Si interface is smaller or similar than at the Ag/organic interface except for the CuPc_12 nm sample.

In the positive mode, RMS values at the interfaces for the Alq_3_30 nm sample are significantly higher than in the negative mode (1.3 and 1.6 nm compared to 0.9 nm or lower). In the middle of the organic layer, roughness is slightly smaller than in the negative mode (1.9 nm compared to 2.3 or 2.6 nm). These values are significantly higher than those for the CuPc_30 nm sample (1.2 nm in the Ag and CuPc layers as well as at the interfaces). For the CuPc_−60 °C sample in the positive mode, roughness at the Ag/CuPc interface is still low (1.1 nm), but it is significantly higher at the CuPc/Si interface (roughness of 2.3 nm). The overall trend is similar for the Alq_3_30 nm and CuPc_−60 °C samples. Lower roughness values throughout the whole sample are only observed for the CuPc_30 nm sample.

For the Alq_3 and CuPc_−60 °C samples, the lowest roughness at the organic/Si interface is always obtained in the negative secondary ion mode, either with or without sample rotation. For the Ag/organic interface, the negative mode with sample rotation yields the lowest roughness and the results of both modes without sample rotation depend on the layer composition. For the CuPc_30 nm in the negative mode, this implies that the roughness at the Ag/CuPc is equal or slightly higher than in the positive mode and roughness at the CuPc/Si interface could even be smaller than what is observed in the positive secondary ion mode.

An explanation for the influence of the secondary ion mode on roughness formation is the incidence angle on the Cameca Sc-Ultra instrument, which changes from about 46° in the negative secondary ion mode to about 64° in the positive secondary ion mode. The angles are given with respect to the surface normal. These angles are caused by the deflection of the primary ion beam in the extraction field of the mass spectrometer and cannot be modified significantly for given analysis conditions.[40] Furthermore, roughness formation has already been reported to be more pronounced for high incidence angles.[41−43] In addition, the difference in mass between light and heavy atoms acts on the impact-induced relocation of surface target atoms, which leads to enhanced roughness formation. This has been observed experimentally for the formation of Si nanodots induced by Mo seeding during Ar^+ irradiation of a silicon surface[44] or the formation of nanocone arrays on an Ar^+ irradiated silicon surface after Fe and Cr incorporation.[45] This concept could also be explained by theory[46] and modeling.[47] In our samples, this same mechanism probably acts between the heavier atoms Ag or Si and the lighter elements in the organic molecules and enhances roughness formation as long as the concentration of a heavier element is above a critical threshold.

In the Experimental Section, the formation of Cs−O hillocks in the Cs^+-sputtered craters after exposure to air has already been mentioned. With our experimental setup, the exposure to air during the transfer of the samples to the AFM instrument cannot be avoided. The formation of these hillocks has been studied thoroughly in a previous paper.[33] However, there are two important results for this study: (i) for the kind of samples studied in this work, the hillocks have only been observed in the organic layers and (ii) the size of the Cs−O droplets depends on the composition and the thickness of the organic layer. For the thin CuPc layers (CuPc_12 nm and CuPc_−60 °C samples) and the Alq_3 layer (Alq_3_30 nm sample), only small droplets form. They are difficult to mask by the procedure described in the Experimental Section, and the smallest droplets cannot be masked successfully: they contribute to the RMS roughness calculated for these three samples and the real roughness during the SIMS measurement, where no such dots are present, is smaller. This is important to consider when comparing the RMS roughness to the interface widths calculated from the SIMS depth profiles.

DISCUSSION

The interface widths calculated from the SIMS depth profiles can only be used to characterize the interface structure of metal−organic multilayered samples when the sputter-induced roughness in the SIMS craters is smaller than the interface roughness developed during sample deposition. Most important for the characterization of organic optoelectronic devices is the characterization of the metal/organic interfaces. The silicon wafer has always the same small roughness, i.e., the real interface width is always small, and the interface widths obtained from the SIMS depth profiles are increased by atomic mixing and sputter-induced roughness. The relation between interface width and roughness is not always obvious. In general, small roughness (0.9 nm for Alq_3_30 nm and 1.0 nm for CuPc_−60 °C) produces also small interface widths of 2.0 and 2.5 nm, respectively. For CuPc_30 nm, a larger interface width of 3.2 nm correlates with a larger roughness of 1.2 nm. It is important to consider that the depth profile for the calculation of interface widths and the craters for AFM measurements were sputtered using different secondary ion polarities resulting in different incident angles of the primary beam and thus different roughness values. As discussed in the previous section, the roughness at the Ag/CuPc interface might be slightly higher, but even then it will stay most probably significantly below the interface widths. Samples CuPc_12 nm and CuPc_48 nm do not seem to follow that rule. At first, they have been prepared on another instrument which may result in different layer properties. In addition, the organic layer of the CuPc_12 nm sample is so thin that the sputter-induced roughness developed at the Ag/CuPc interface has not been significantly reduced before reaching the CuPc/Si interface. For sample CuPc_48 nm, the organic layer is much thicker which leads to a much decreased roughness at the CuPc/Si interface. In both situations, preferential sputter rates at the first interface producing roughness compete with smoothening during the sputtering of the organic layer (low Ag concentration).

For the Ag/organic interfaces, the RMS roughness in the negative secondary ion mode stays for all samples below 2 nm. In this same mode, it produces the lowest roughness values and as such it has been chosen to calculate the interface widths. For the CuPc_48 nm and CuPc_−60 °C samples, the roughness is close to 2 nm and for the other samples it is even as low as 0.9 nm −1.2 nm. At the organic/Si interfaces, roughness is even lower with a maximum of 1.3 nm for the CuPc_12 nm sample,

dx.doi.org/10.1021/ac302939m | Anal. Chem. 2013, 85, 381−388

close to 1 nm for the CuPc_−60 °C (1.0 nm) and CuPc_30 nm (1.2 nm measured in positive mode) samples, and even below 1 nm for the Alq_3_30 nm (0.9 nm) and CuPc_48 nm (0.5 nm) samples. All values given here are for the negative secondary ion mode without sample rotation during SIMS analysis. They are also much smaller than the interface widths determined from the SIMS depth profiles, implying that SIMS depth profiling can be used to characterize interface structure and widths of organic optoelectronic devices. The Alq_3_30 nm and CuPc_−60 °C samples present the smallest interface widths with 3.6 and 3.5 nm, respectively. Cooling the substrate during sample deposition was expected to reduce roughness. Alq_3 seems to lead to smoother films than CuPc. For the remaining CuPc samples, the interface widths increase with layer thickness, indicating that surface roughness during the deposition process develops continuously, at least for the studied samples. The choice of the instrument for sample deposition, i.e., the exact deposition conditions, is also critical for the interface widths, the Superlattice system leading to somewhat more important roughness than the Angstrom system.

CONCLUSIONS

Interface structures in organic optoelectronic devices are of utmost importance as they define the properties of the devices. In this study, the interest of low-energy SIMS depth profiling for the characterization of interface structures in organic optoelectronic devices was investigated. Interface widths can only be calculated from the depth profiles if sputter-induced roughness in the SIMS craters can be controlled and remains significantly smaller than the real interface width. When using 500 eV Cs^+ bombardment on the Cameca Sc-Ultra instrument and analyzing negative secondary ions, the RMS roughness at the Ag/organic interfaces varied between 0.9 and 1.9 nm. These values are much smaller than the interface widths calculated at the interfaces of the corresponding samples and which change between 1.8 and 5.9 nm. Thus, when using these analysis conditions, interface characterization is not limited by roughness formation. In addition, the difference in roughness formation between negative and positive secondary ion mode could be related to the different impact angles which cannot be varied independently from the analysis conditions.

The results show that SIMS can be used to characterize interface structures in organic optoelectronic devices and help to correlate interface structures to sample preparation conditions and device properties. The depth profiles reveal that the interface widths depend on the composition and thickness of the organic layer, and to a lesser degree on the instrument used during the deposition process. Alq_3 leads to smoother films than CuPc and interface roughness increases with film thickness. Changing substrate temperature revealed to be an efficient method to change interface properties. The smoothest films have been obtained at −60 °C. These specific results have been obtained at 500 eV on a Cameca Sc-Ultra instrument using Cs^+ bombardment and cannot be generalized to other analysis conditions as they may alter roughness formation and atomic mixing significantly.

The SIMS depth profiles show also an important diffusion of Ag into the organic layer. This diffusion could happen during the deposition process or/and during SIMS analysis. This aspect will be investigated in a forthcoming paper.

AUTHOR INFORMATION

Corresponding Author

*E-mail: philipp@lippmann.lu.

Notes

The authors declare no competing financial interest.

ACKNOWLEDGMENTS

The present project is supported by the National Research Fund, Luxembourg (Grant NSF-FNR-MAT-07-01) and the U.S. National Science Foundation (Grant NSF-DMR 0806867). We thank Yansha Jin, Samanthule Nola, and other students in Max Shtein's group at Michigan University for support in sample preparation. We thank Patrick Grysan for help with the AFM measurements. We also thank Susanne Siebentritt for interesting discussions.

REFERENCES

(1) Benninghoven, A. *Angew. Chem., Int. Ed.* **1994**, *33* (10), 1023−1043.
(2) Zalm, P. C. *Rep. Prog. Phys.* **1995**, *58*, 1321.
(3) Adriaens, A.; Van Vaeck, L.; Adams, F. *Mass Spectrom. Rev.* **1999**, *18* (1), 48−81.
(4) Mahoney, C. M. *Mass Spectrom. Rev.* **2010**, *29* (2), 247−293.
(5) Fletcher, J. S.; Lockyer, N. P.; Vickerman, J. C. *Mass Spectrom. Rev.* **2011**, *30* (1), 142−174.
(6) Shard, A. G.; Brewer, P. J.; Green, F. M.; Gilmore, I. S. *Surf. Interface Anal.* **2007**, *39*, 294−298.
(7) Shard, A. G.; Green, F. M.; Brewer, P. J.; Seah, M. P.; Gilmore, I. S. *J. Phys. Chem. B* **2008**, *112* (9), 2596−2605.
(8) Sostarecz, A. G.; Sun, S.; Szakal, C.; Wucher, A.; Winograd, N. *Appl. Surf. Sci.* **2004**, 231−232.
(9) Szakal, C.; Sun, S.; Wucher, A.; Winograd, N. *Appl. Surf. Sci.* **2004**, *231*−*232*, 183−185.
(10) Baker, M. J.; Fletcher, J. S.; Jungnickel, H.; Lockyer, N. P.; Vickerman, J. C. *Appl. Surf. Sci.* **2006**, *252*, 6731−6733.
(11) Fletcher, J. S.; Conlan, X. A.; Jones, E. A.; Biddulph, G.; Lockyer, N. P.; Vickerman, J. C. *Anal. Chem.* **2006**, *78* (6), 1827−1831.
(12) Brunelle, A.; Della-Negra, S.; Deprun, C.; Depauw, J.; Hakansson, P.; Jacquet, D.; le Beyec, Y.; Pautrat, M. *Int. J. Mass Spectrom. Ion Processes* **1997**, *164*, 193−200.
(13) Beyec, Y. L. *Int. J. Mass Spectrom. Ion Processes* **1998**, *174*, 101.
(14) Brunelle, A.; Della-Negra, S.; Depauw, J.; Jacquet, D.; Beyec, Y. L.; Pautrat, M.; Baudin, K.; Andersen, H. H. *Phys. Rev. A* **2001**, *63*, 22902.
(15) Harris, R. D.; Baker, W. S.; Stipdonk, M. J. V.; Crooks, R. M.; Schweikert, E. A. *Rapid Commun. Mass Spectrom.* **1999**, *13*, 1374−1380.
(16) Rickman, R. D.; Verkhoturov, S. V.; Hager, G. J.; Schweikert, E. A. *Int. J. Mass Spectrom.* **2005**, *245*, 48−52.
(17) Novikov, A.; Caroff, M.; Della-Negra, S.; Depauw, J.; Fallavier, M.; le Beyec, Y.; Pautrat, M.; Schultz, J. A.; Tempez, A.; Woods, A. S. *Rapid Commun. Mass Spectrom.* **2005**, *19*, 1851−1857.
(18) Mahoney, C. M.; Roberson, S. V.; Gillen, G. *Anal. Chem.* **2004**, *76* (11), 3199−3207.
(19) Wagner, M. S.; Lenghaus, K.; Gillen, G.; Tarlov, M. J. *Appl. Surf. Sci.* **2006**, *253*, 2603−2610.
(20) Touboul, D.; Kollmer, F.; Niehuis, E.; Brunelle, A.; Laprevote, O. *J. Am. Soc. Mass Spectrom.* **2005**, *16* (10), 1608−1618.
(21) Ninomiya, S.; Ichiki, K.; Yamada, H.; Nakata, Y.; Seki, T.; Aoki, T.; Matsuo, J. *Rapid Commun. Mass Spectrom.* **2009**, *23* (11), 1601−1606.
(22) Ninomiya, S.; Ichiki, K.; Yamada, H.; Nakata, Y.; Seki, T.; Aoki, T.; Matsuo, J. *Rapid Commun. Mass Spectrom.* **2009**, *23* (20), 3264−3268.
(23) Lee, J. L. S.; Ninomiya, S.; Matsuo, J.; Gilmore, I. S.; Seah, M. P.; Shard, A. G. *Anal. Chem.* **2009**, *82* (1), 98−105.

(24) Chanbasha, A. R.; Wee, A. T. S. *Appl. Surf. Sci.* **2006**, *252*, 7243−7246.
(25) Py, M.; Barnes, J. P.; Charbonneau, M.; Tiron, R.; Buckley, J. *Surf. Interface Anal.* **2011**, *43* (1−2), 179−182.
(26) Song, W.; Li, Z.; So, S. K.; Qiu, Y.; Zhu, Y.; Cao, L. *Surf. Interface Anal.* **2001**, *32* (1), 102−105.
(27) Nonaka, T.; Mori, Y.; Nagai, N.; Nakagawa, Y.; Saeda, M.; Takahagi, T.; Ishitani, A. *Thin Solid Films* **1994**, *239* (2), 214−219.
(28) Mine, N.; Douhard, B.; Brison, J.; Houssiau, L. *Rapid Commun. Mass Spectrom.* **2007**, *21* (16), 2680−2684.
(29) Cramer, H. G.; Grehl, T.; Kollmer, F.; Moellers, R.; Niehuis, E.; Rading, D. *Appl. Surf. Sci.* **2008**, *255* (4), 966−969.
(30) Jin, Y.; Yadav, A.; Sun, K.; Pipe, K. P.; Shtein, M. *Appl. Phys. Lett.* **2011**, *98* (9), 093305.
(31) An, K. H.; Shtein, M.; Pipe, K. P. *Opt. Express* **2010**, *18* (5), 4041−4048.
(32) Cirlin, E. H.; Vajo, J. J.; Hasenberg, T. C.; Hauenstein, R. J. *J. Vac. Sci. Technol. A* **1990**, *8* (6), 4101.
(33) Ngo, K. Q.; Philipp, P.; Kieffer, J.; Wirtz, T. *Surf. Sci.* **2012**, *606* (15−16), 1244−1251.
(34) Ngo, K. Q.; Philipp, P.; Jin, Y.; Morris, S. E.; Shtein, M.; Kieffer, J.; Wirtz, T. *Surf. Interface Anal.* **2011**, *43* (1−2), 88−91.
(35) Jiang, Z. X.; Kim, K.; Lerma, J.; Sieloff, D.; Tseng, H.; Hegde, R. I.; Luo, T. Y.; Yang, J. Y.; Triyoso, D. H.; Tobin, P. J. *Appl. Surf. Sci.* **2006**, *252*, 7172−7175.
(36) Wittmaack, K. *J. Appl. Phys.* **1982**, *53* (7), 4817.
(37) Dowsett, M. G.; Barlow, R. D. *Anal. Chim. Acta* **1994**, *297*, 253.
(38) Mansilla, C.; Philipp, P.; Wirtz, T. *Nucl. Instrum. Methods Phys. Res. B* **2011**, *269* (9), 905−908.
(39) Mansilla, C.; Philipp, P.; Wirtz, T. *Surf. Interface Anal.* **2012**, DOI: 10.1002/sia.5054.
(40) Cameca Sc-Ultra user manual.
(41) Kataoka, Y.; Shigeno, M.; Tada, Y.; Yamazaki, K.; Kase, M. *FUJITSU Sci. Tech. J.* **2002**, *38* (1), 69.
(42) van der Heide, P. A. W.; Bennett, J. *Appl. Surf. Sci.* **2003**, *203*, 156−159.
(43) Kataoka, Y.; Yamazaki, K.; Shigeno, M.; Tada, Y.; Wittmaack, K. *Appl. Surf. Sci.* **2003**, *203*−*204*, 43−47.
(44) Ozaydin, G.; Ozcan, A. S.; Wang, Y.; Ludwig, K. F.; Zhou, H.; Headrick, R. L.; Siddons, D. P. *Appl. Phys. Lett.* **2005**, *87* (16), 163104-3.
(45) Jing, Z.; Hildebrandt, M.; Ming, L. *J. Appl. Phys.* **2011**, *109* (5), 053513−053515.
(46) Madi, C. S.; Anzenberg, E.; Ludwig, K. F., Jr.; Aziz, M. J. *Phys. Rev. Lett.* **2011**, *106* (6), 066101.
(47) Norris, S. A.; Samela, J.; Bukonte, L.; Backman, M.; Djurabekova, F.; Nordlund, K.; Madi, C. S.; Brenner, M. P.; Aziz, M. J. *Nat. Commun.* **2011**, *2*, 276.